Title
Three-dimensional architectures constructed using two-dimensional nanosheets

Journal
Science China Chemistry, 58(12)

ISSN
1674-7291

Authors
Li, Haoyi
Wang, Xun

Publication Date
2015-12-01

DOI
10.1007/s11426-015-5511-x

Peer reviewed

SCIENCE CHINA
Chemistry

• MINI REVIEWS •

December 2015 Vol.58 No.12: 1792–1799
doi: 10.1007/s11426-015-5511-x

Three-dimensional architectures constructed using two-dimensional nanosheets

Haoyi Li & Xun Wang*

Department of Chemistry, Tsinghua University, Beijing 100084, China

Received October 23, 2015; accepted November 4, 2015; published online November 16, 2015

Two-dimensional (2D) nanomaterials such as transition metal dichalcogenides (TMDs) and graphene have attracted extensive interest as emergent materials, owing to their excellent properties that favor their future use in electronic devices, catalysis, optics, and biological- or energy-relevant areas. However, 2D nanosheets tend to easily restack and condense, which weakens their performance in many of these applications. Assembling these 2D nanosheets as building blocks for three-dimensional (3D) architectures not only maintains the intrinsic performances of the 2D nanostructures but also synergistically makes use of the advantages of the 3D microstructures to improve the overall material properties. In this critical review, we will highlight recent developments of sundry 2D nanosheet-assembled 3D architectures, including their design, synthesis, and potential applications. Their controllable syntheses, novel structures, and potential applications will be systematically explained, analyzed, and summarized. In the end, we will offer some perspective on the challenges facing future advancement of this field.

3D architectures, 2D nanosheets, restack, assembly

1 Introduction

The term "nano" has seen extensive use in the sciences and technologies developed in the 21st century [1–5]. Scientific research into nanomaterials and nanotechnology has increased rapidly in this period, and shows no signs of slowing down [6–20]. Compared to their bulk counterparts, nanomaterials often exhibit very different properties, such as surface effects, small size effects, quantum confinement effects, and show a series of unusual behaviors in terms of electronics, optics, magnetics, thermal conductivity, and more [21–28]. Studies detailing new concepts, controllable methodologies, novel structures, and comprehensive applications of these nanomaterials are plentiful [29–44].

In recent years, 2D layered nanocrystals, such as graphene [45–48], TMDs [49–51], and other inorganic analogues [48,52–56], have received tremendous attention owing to their superior electronic, optical, and mechanical properties. A large number of methods have been demonstrated for the controllable synthesis of 2D layered materials, such as chemical vapor deposition (CVD) growth [57], wet chemical synthesis [5], exfoliation [45], and electrochemical synthesis [58]. Nevertheless, in the process of their synthesis and application, 2D nanosheets preferentially restack on account of the strong interlayer Van Der Waals interactions and high surface energy [59] of these materials, which gravely decrease their performance in various applications [60,61]. When 2D nanostructures restack in this manner, the specific surface area decreases and the mass and electron transport kinetics markedly decrease [62], which dramatically compromises the material's performance. To solve this problem and retain the high specific surface areas and fast electron transport of layered structures, an effective approach has been created, where 2D nanosheets are assembled as building blocks for 3D architectures [63–68]. Not only can we make full use of the advantages of 2D layered structures, but 3D assemblies and architectures can also

*Corresponding author (email: wangxun@mail.tsinghua.edu.cn)

provide their own advantages, such as larger surface area, light weight, high mechanical strength, and higher electrical conductivity [62,69]. Therefore, the assembly of 2D nanoplates into 3D microscopic or even macroscopic architectures is a promising field.

However, 3D assemblies and architectures have seen relatively little research attention, even though they have great significance pertaining to mass production and various practical applications [69]. In the fields of electronic and optoelectronic devices, sensors, and electrochemical energy devices, 3D graphene architectures have shown potential in preliminary applications at high production levels. Although several high quality reviews on 3D graphene assemblies have been published [69–71], a review of recently developed transition metal dichalcogenide (TMD) nanosheet-assembled 3D structures does not exist. This review primarily focuses on TMD nanosheet-assembled 3D architectures and other inorganic assemblies. Here, we summarize the recent achievements in design and controllable synthesis and give an overview of the potential applications of these 3D materials. The key advantages of these 3D structures compared to 2D nanoplates restacking are emphasized. We believe that the viewpoints provided in this review can pave the way to develop new 3D architectures and assemblies for future applications.

2 Novel design and controllable 3D assemblies synthesis

Since graphene was first directly exfoliated from graphite by Novoselov and Geim in 2004 [45], 2D layered materials have piqued the interest of chemists, physicists and material scientists. In the same vein, TMDs have received similar attention. Generally speaking, TMDs are a series of materials with the formula MX_2, where M represents a transition metal element and X is a chalcogen. In terms of molecular structure, these materials have the form X–M–X, where the metal atoms are in the center plane and the planes of the chalcogen atoms are separated by the metal atom plane [72], as shown in Figure 1(a). Layered TMDs such as MoS_2, WS_2, and WSe_2 have been further explored in terms of systematic fabrication and characterization, showing a wide range of beneficial electronic, optical, chemical and thermal properties [49–51,73–75].

MoS_2 has a mobility more than 200 $cm^2/(V\ s)$ and exhibits room-temperature current on/off ratios of 10^8 and ultralow standby power dissipation, making it a promising candidate for use in energy-related next-generation materials, particularly in transistors. Monolayer or multi-layer thin flakes of MoS_2 can be synthesized using CVD or mechanical cleavage from the bulk crystal [49,72–74] (Figure 1(b–d)). However, single layer 2D materials (including graphene and TMDs) prefer to aggregate or restack in these applications, especially during repetitive cycling of electrochemical processes, owing to Van Der Waals interactions. This results in the loss of the active sites regardless of whether or not the reaction takes place on the surface or on the edge sites [10], negatively impacting the desired properties [60]. This is but one example of the impact that restacking or aggregation of the 2D layered structures has.

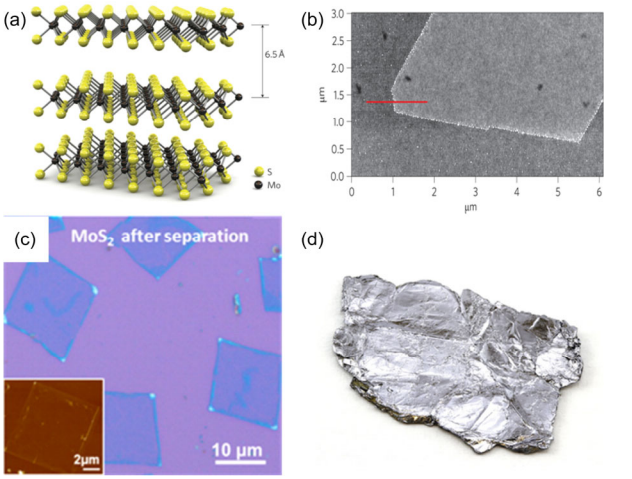

Figure 1 (a) 3D representation of the structure of a typical MX_2 material, with the chalcogen atoms (X) in yellow and the metal atoms (M) in grey; (b) atomic force microscope (AFM) image of a single layer of MoS_2; (c) optical and AFM images (insets) of MoS_2 bilayer plates; (d) 1 cm-length bulk crystal of MoS_2. Figures reproduced with permission from Ref. [73] (a, b), [74] (c) and [72] (d). (color online)

Assembling 2D nanosheets into building blocks of desirable 3D architectures is an effective way to solve the restacking problem and to help further realize the possible applications of nanomaterials. These 3D assemblies exhibit a high specific surface area and porous structures, both of which are beneficial in exposing the active sites for use in catalysis and electrode materials. At the same time, these hollow structures can provide void spaces that effectively buffer volume variation during the application. Compared to the restacking structures, well-defined 3D architectures have faster mass and electron transfer for use in electric nanodevices and electrocatalysis [64,65,76,77].

2.1 Graphene-based macroscopic assembly

As one of the most well-known 2D layered materials, graphene has facilitated recent research of 2D nanomaterials and has been used to construct current 3D macroscopic architectures [63,67–71]. Tang *et al.* [63] have demonstrated 3D macrostructures (Figure 2(D, E)) assembled using single-layered graphene oxide (GO) (Figure 2(B, C)) with a hydrothermal method for the first time. These 3D GO assemblies are lightweight and have a large surface area, excellent mechanical strength, high conductivity and high strength endurance. They were subsequently combined with a series of noble-metal nanocrystals, which might result in some interesting properties. It has been demonstrated that

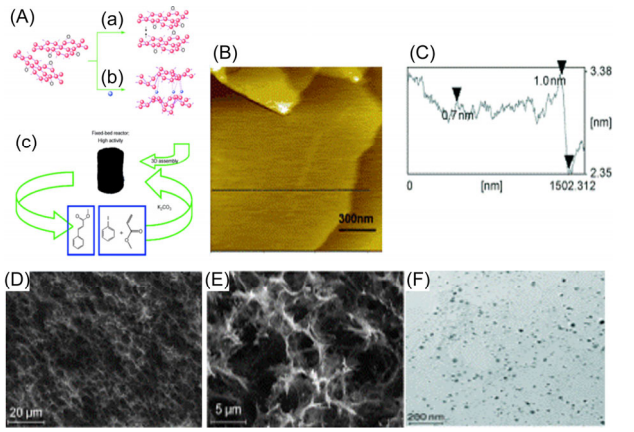

Figure 2 (A) Schematic representation of the assembly of (a) GO sheets and (b) GO sheets with a noble metal (e.g., Pd); (c) schematic of a Heck reaction in a fixed-bed reactor; (B) AFM image of a graphene oxide monolayer, where the line indicates the direction of the height profile in (C); (D) scanning electron microscopy (SEM) image of the sample prepared when the concentration of the graphene oxide suspension was 0.1 mg/mL; (E) SEM image of the 3D structure containing Au; (F) transmission electron microscope (TEM) image of graphene oxide bearing Pd nano-particles. Figure reproduced with permission from Ref. [63]. (color online)

Pd-embedded assemblies (Figure 2(F)) showed excellent catalytic activity and selectivity for the Heck reaction (Figure 2(A)). This material has potential for use in catalysis associated with large-scale production.

2.2 MoS_2- or $MoSe_2$-based 3D tubular architectures

Our group has previously reported on the assembly of 2D nanosheet-based materials into designed 3D architectures. Wang *et al*. [64] developed a simple approach to synthesize 3D tubular architectures of MoS_2 with tunable sizes as established by its layers. The controllable synthesis was implemented in a mixed solution of ethanol and octylamine, in which ethanol was regarded as a poor solvent to adjust the morphology and size of the production. As shown in Figure 3(a, b), the central hollow structure and porous and uneven tube walls can be clearly seen. According to the rim image of the tubes (Figure 3(c)), the tube is clearly assembled from MoS_2 layers. The center hollow and porous structures can provide more defect sites and a large surface area, which means that this structure has a higher interface activity, and facilitates the transport and storage of ions and mass.

In addition, Yang *et al*. [65] have reported a facile method to synthesize hierarchical $MoSe_2$ and S-doped $MoSe_{2-x}$ 3D assemblies. The worm-like $MoSe_2$ and the tubular S-doped $MoSe_{2-x}$ structures are shown in Figure 4(a, c). The edge images of the productions (Figure 4(b)) exhibit that the $MoSe_2$ or S-doped $MoSe_{2-x}$ nanosheets are the building blocks of the 3D trusses and the random distribution of nanoplates has a tendency to expose more edge active sites for practical applications. It is apparent that MoS_2 nanosheets tend to arrange in a disordered manner during 3D assembly, which is the natural character of MoS_2 nanosheets. As shown in Figure 4(d), there are a few unsaturated sites and active sites on the S-doped $MoSe_{2-x}$ nanoplates (100) basal plane, which promote the electrochemical hydrogen evolution process.

Besides, Zhuo *et al*. [78] have reported hierarchical nanosheet-based MoS_2 nanotubes (Figure 5(a, b)) synthesized using an anion-exchange approach (Figure 5(c)). These tubular analogues have a high specific surface area as well as mesopores in the shell, which facilitate the reversible transport of mass and electrons and the exposing of active sites for photo-electrochemical catalysis.

2.3 MoS_2-based 3D core-shell hollow structures

While it is expected that MoS_2 assemblies form hollow structures, there is another class of hollow architectures that are microsphere analogues. For example, Lou and coworkers [76] have reported three types of hollow structures assembled by MoS_2 nanosheets. The first one is MoS_2 hierarchical microboxes (Figure 6(a, b)), which were obtained using a hydrothermal process with $MnCO_3$ microboxes as a

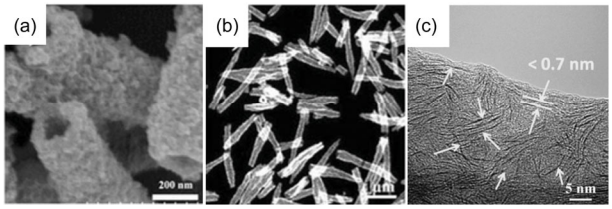

Figure 3 (a) SEM and (b) STEM (scanning transmission electron microscope) images of the 3D architectures assembled from single-layered MoS_2; (c) HRTEM (high resolution transmission electron microscope) image of the rim of the MoS_2 tube. Figure reproduced with permission from Ref. [64].

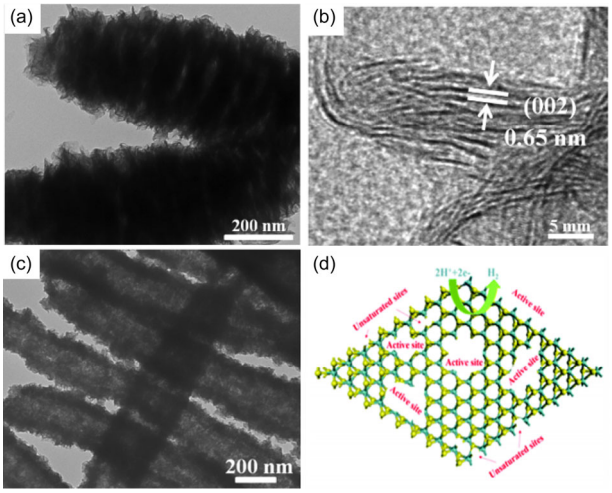

Figure 4 (a) TEM image of $MoSe_2$ nanocaterpillars; (b) HRTEM analysis taken from the edge area of (a); (c) TEM image of S-doped $MoSe_{2-x}$ nanotubes; (d) schematic illustration of the unsaturated edges on the nanosheet (100) basal plane and edge-rich ultrathin nanosheets for hydrogen evolution reaction (HER). Figure reproduced with permission from Ref. [65]. (color online)

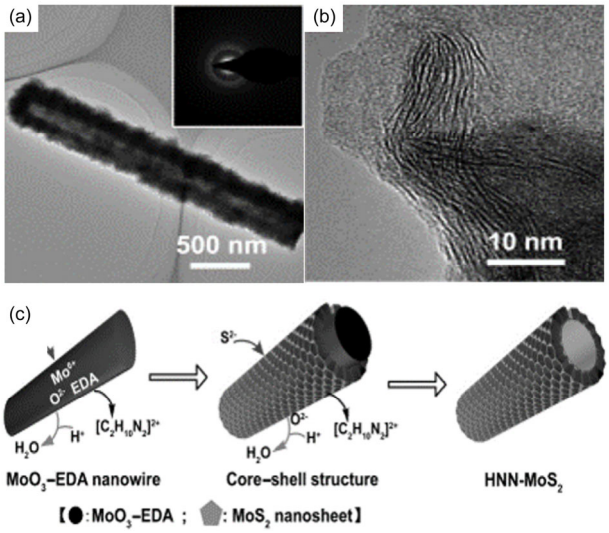

Figure 5 (a) TEM image and (b) HRTEM image of a hierarchical nanosheet-based MoS_2 nanotube; (c) schematic representation of the synthesis of hierarchical nanosheet-based MoS_2 nanotubes (HNN-MoS_2; cross-section view) through the anion-exchange reaction of the inorganic-organic MoO_3-EDA hybrid nanowires with S^{2-} at elevated temperatures. Figure reproduced with permission from Ref. [78].

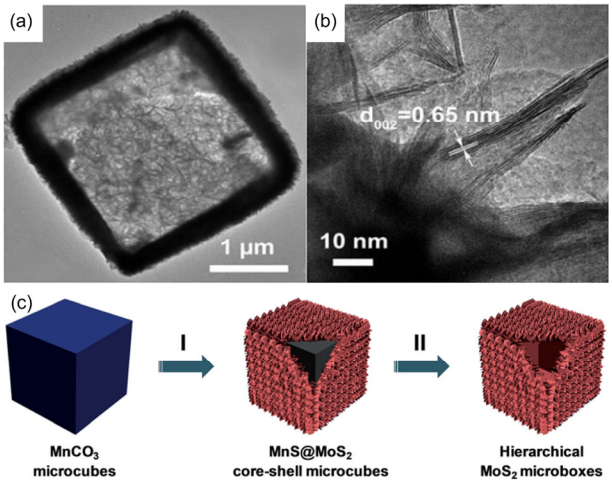

Figure 6 (a) TEM image of hierarchical MoS_2 microboxes; (b) HRTEM image taken from the edge area of (a); (c) schematic illustration of the template-assisted formation of hierarchical MoS_2 microboxes. I: $MnCO_3$ microcube templates are coated uniformly with MoS_2 nanosheets; II: the microcube templates are removed by washing with HCl to form hierarchical MoS_2 microboxes. Figure reproduced with permission from Ref. [51]. (color online)

template (Figure 6(c)). The second type is MoS_2 hierarchical microspheres (Figure 7(a, b)), which were produced using a wet chemical method with polystyrene microspheres as a template [77]. The last one is hierarchical MoS_2 shells supported on carbon spheres (Figure 7(c, d)), which were synthesized by a facile hydrothermal method assisted with carbon spheres [79]. These structures have large specific surface areas, with abundant active sites for catalysis and large contact areas across the interface for use in electrode materials. The center hollow structures can offer void spaces that effectively buffer the volume variation during the application process, especially in Li ion charge/discharge processes for Li ion batteries.

2.4 ZnS-based 3D assemblies

It is also possible for other TMD materials to form 3D assemblies. For instance, in our group, Wang *et al*. [66] have demonstrated the construction of ZnS nanosheet-based hybrid superlattices with rod and tube architectures and tunable periodic distances between the layers (Figure 8(b–e)). This work illustrated a new design for synthesizing such assemblies. By utilizing alkyl amines as structure-directing agents, highly ordered arrangements of ZnS nanosheets were exhibited in superstructures with either rods or tubes compared to MoS_2 3D architectures mentioned above (Figure 8(a)). Through employing different amines with different chain length, superlattices with different layer spacings can be obtained, and the superstructures with shortest interlayer spacings show the best performance when used in photoelectrochemical cells due to having faster electron transport. The large active surface area of nanosheet building blocks

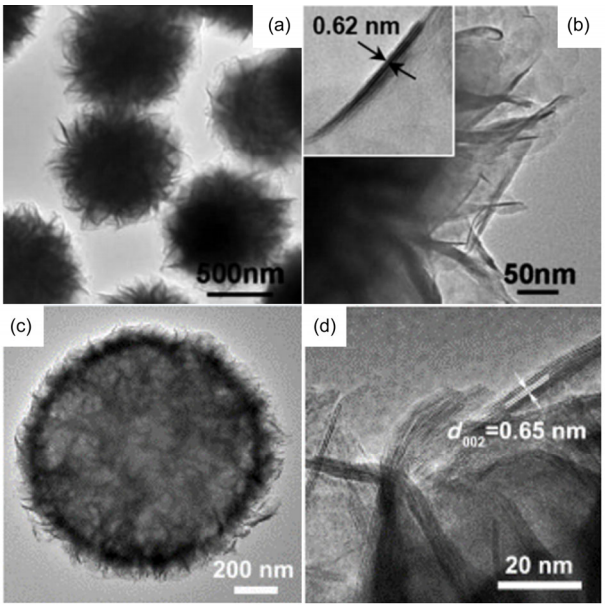

Figure 7 (a) TEM image of the MoS_2 microspheres; (b) HRTEM image taken from the edge area of (a); (c) TEM image of hierarchical C@MoS_2 microspheres; (d) HRTEM image taken from the edge area of (c). Figure reproduced with permission from Ref. [77] (a, b) and [79] (c, d).

and the ordered superstructures that can effectively avoid agglomeration and restacking are the two key factors in the excellent performance of these materials in photo-electrochemical catalysis.

3 Electrochemical properties

TMDs are a class of materials with high potential for use in

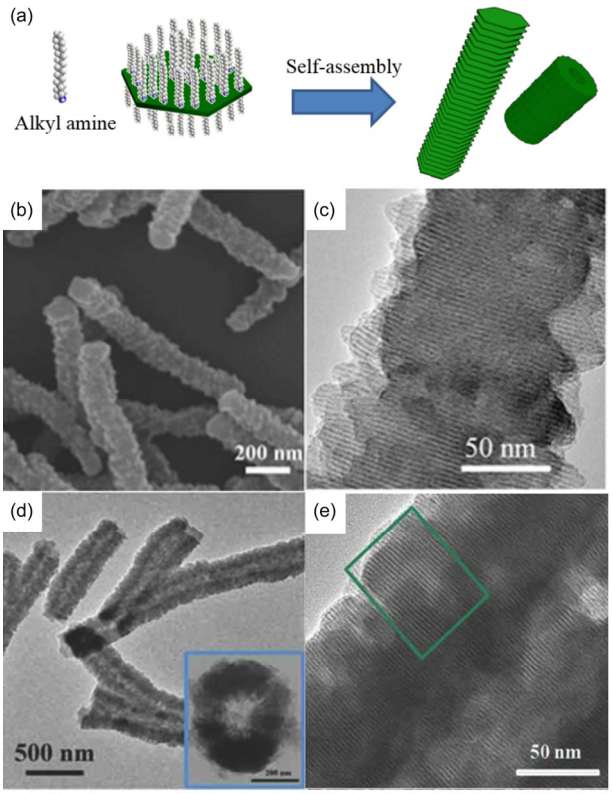

Figure 8 (a) Schematic representation of the formation of ZnS ultrathin nanosheet-based hybrid superlattices with rod-like and tubular morphologies; (b) typical SEM image of the assemblies; (c) TEM image of the ZnS hybrid super- lattices with rod architecture; (d, e) TEM images of the ZnS hybrid superlattices with tube architectures.The inset of (d) is a sectional view of a short tube, showing clearly the cavity structures. Figure reproduced with permission from Ref. [66]. (color online)

catalysis, electronic devices, and batteries. The goal of engineering functional 3D architectures from 2D TMD nanosheets with well-defined morphologies is to optimize their properties and avoid shortages, thereby achieving better application performance. In this portion, we will concentrate on discussing the effect of 3D assemblies and architectures on these applications, highlighting the best-performing 3D structures.

3.1 Hollow structures

As mentioned previously, MoS_2 assemblies can form hollow structures through self-assembly or template-assisted methods. These hollow structures could potentially be used as the electrode materials of lithium-ion batteries. During the charge-discharge process, the electrode materials go through the process of lithium ion insertion and removal, and the volume of the electrode materials expands and shrinks. As a result, hollow structures provide large void spacings that buffer the volume variation accompanying the charge-discharge process, leading to improved stability performance [64,76,77].

Lou and co-workers [76] examined the above process in greater detail. As shown in Figure 9(c), hierarchical MoS_2 hollow micro-boxes (Figure 9(a)) exhibit high specific capacity and enhanced cycling stability for lithium-ion batteries. After 50 cycles, a high discharge capacity of ~900 mA h/g can be maintained, while the MoS_2 microparticles can only maintain 600 mA h/g, which is a much faster capacity fading under identical test conditions. Moreover, the hierarchical MoS_2 microboxes also exhibit a coulombic efficiency greater than 95% from the second cycle onwards. The large center space of the hollow structure effectively buffers the mechanical stress caused by volume changes during lithium insertion and removal. At the same time, hierarchical MoS_2 microboxes show large surface areas of 34 m^2/g in a N_2 adsorption-desorption isotherm spectrum (Figure 9(b)), which is a consequence of the hollow structure and leads to enhanced stability. Other hollow 3D assemblies of MoS_2 analogues also show fantastic stability performance of lithium-ion batteries [64,65,77,78].

3.2 Uneven and porous surfaces

Owing to the disordered arrangement of the MoS_2 nanosheet building blocks, 3D architectures generally have uneven and porous surfaces [64], as shown in Figure 10(A). This feature imparts the MoS_2 nanosheet-assembled tubes with large specific surface areas (96 m^2/g, Figure 10(B)),

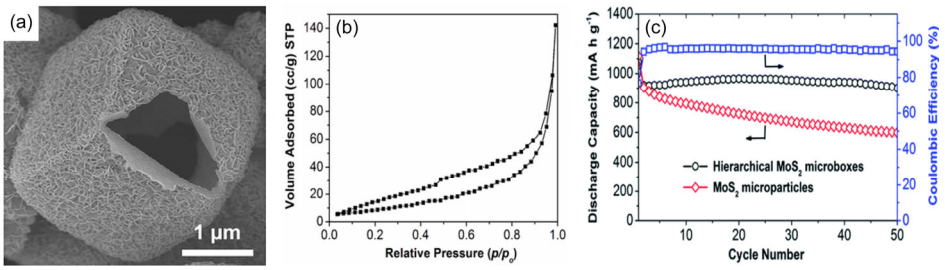

Figure 9 (a) FE-SEM (field emission scanning electron microscope) image of hierarchical MoS_2 microboxes; (b) N_2 adsorption-desorption isotherm of hierarchical MoS_2 microboxes; (c) cycling performance of annealed hierarchical MoS_2 microboxes and MoS_2 microparticles, and coulombic efficiency of annealed hierarchical MoS_2 microboxes within a voltage range of 0.05–3.0 V vs. Li/Li^+ at a current density of 100 mA/g. Figure reproduced with permission from Ref. [76]. (color online)

which can provide more interfaces with active sites for charge-discharge processes. At the same time, uneven and porous surfaces lead to a large electrode-electrolyte contact area for high Li^+ ion flux across the interface. Compared to MoS_2 nanosheets and commercial MoS_2, 3D assembled MoS_2 tubes exhibit better stability after 50 cycles (Figure 10(C)). Moreover, a large surface area can offer more active sites for water splitting, both in terms of photocurrent response and electrochemical hydrogen evolution [76].

MoS_2 and its analogues are also interesting electrode materials for future use in electrochemical hydrogen evolution reaction (HER) systems [10,16, 80,81]. The MoS_2 micro-boxes (Figure 5(a)) were evaluated for their HER properties, and exhibited clear superiority over the MoS_2 nanosheet aggregated microparticles [76] (Figure 11). The specific surface area was calculated to be 15 m^2/g using the Brunauer-Emmett-Teller (BET) method (Figure 11(b)). This result confirms that the hierarchical MoS_2 architectures have good electronic and ionic conductivity and are more active on the interface, which contributes to the vastly improved electrochemical performance.

4 Conclusions and perspectives

Due to the problem of restacking 2D TMD layers in the process of the practical applications, many efforts have been devoted to develop 3D TMD architectures in order to avoid aggregation of nanosheets. There is also an ongoing challenge to form hollow and uneven structures that increase the interface with active sites of catalysis and buffering the mechanical stress of volume variation. At present, many 3D TMD assemblies and architectures have been synthesized with controlled, well-designed strategies. The structural features and electrochemical properties (especially Li-ion battery performance) have been summarized and analyzed in detail. The key advantages of the 3D architectures applied in electrocatalytic fields have been emphasized, as well as the performance improvements that they provide.

There are still some challenges that exist in the field of 3D TMD assemblies. On the one hand, among the reported 3D architectures, MoS_2 has the best overall performance, implying that more research efforts should be devoted to further study of the other 3D TMD assemblies in the literature. On the other hand, the 3D TMD assemblies synthesized today are mainly used as electrode materials, which is a limited scope for the currently know 3D TMD architectures. Additional properties pertaining to energy storage, thermoelectric devices, sensors, and so on, merit study in order to expand the practical applications of these assemblies. One possible direction lies in the formation of 3D TMD assemblies from different types of 2D nanomaterials towards the realization of high performance materials for use in various applications.

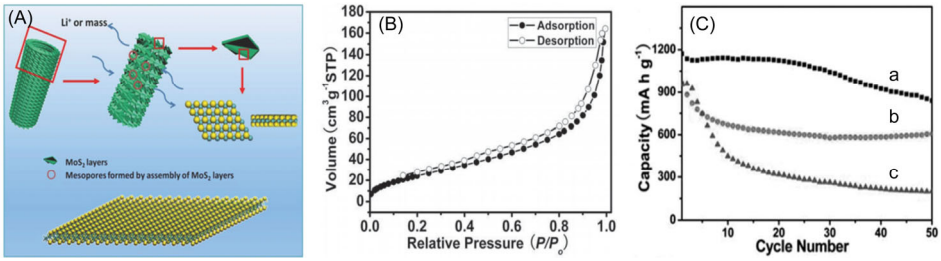

Figure 10 (A) Schematic representation of 3D architectures assembled from single-layered MoS_2 (top panel). The mesopores formed by assembly of MoS_2 layers facilitate the transport of Li ion and mass in LIBs, resulting enhanced performances. (B) N_2 adsorption/desorption isotherms of the assembled tubes. (C) Cycling performance for (a) assembled MoS_2 tubes, (b) nanosheets, and (c) commercial MoS_2 powder. The tests are conducted between 0.01–3.0 V at a current density of 100 mA/g. Figure reproduced with permission from Ref. [64]. (color online)

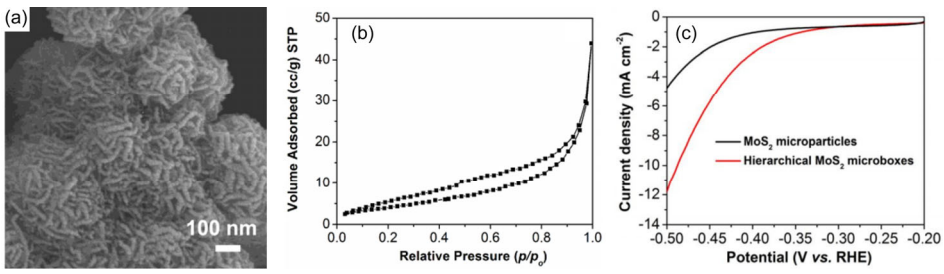

Figure 11 (a) FESEM image of the MoS_2 microparticles obtained without adding $MnCO_3$ microcube templates; (b) N_2 adsorption-desorption isotherm of MoS_2 microparticles; (c) polarization curves for the hierarchical MoS_2 microboxes and MoS_2 microparticles. Figure reproduced with permission from Ref. [76]. (color online)

This work was supported by the National Natural Science Foundation of China (21431003, 91127040, 21221062), and the State Key Project of Fundamental Research for Nanoscience and Nanotechnology (2011CB-932402).

1 Iijima S. Helical microtubules of graphitic carbon. *Nature*, 1991, 354: 56–58
2 Murray C, Kagan C, Bawendi M. Self-organization of CdSe nanocrystallites into three-dimensional quantum dot superlattices. *Science*, 1995, 270: 1335–1338
3 Peng X, Manna L, Yang W, Wickham J, Scher E, Kadavanich A, Alivisatos AP. Shape control of CdSe nanocrystals. *Nature*, 2000, 404: 59–61
4 Pan Z, Dai Z, Wang Z. Nanobelts of semiconducting oxides. *Science*, 2001, 291: 1947–1949
5 Wang X, Zhuang J, Peng Q, Li Y. A general strategy for nanocrystal synthesis. *Nature*, 2005, 437: 121–124
6 Zhang L, Zhou X, Chu T. Preparation and evaluation of Fe_3O_4-core@Ag-shell nanoeggs for the development of fingerprints. *Sci China Chem*, 2013, 56: 551–556
7 Xiong B, Wang C, Luo J, Chen B, Zhou B, Zhu Z. Highly-ordered dye-sensitized TiO_2 nanotube arrays film used for improving photoelectrochemical electrodes. *Sci China Chem*, 2013, 56: 101–105
8 Han L, Ye T, Lv L, Wang K, Wei X, Li X, Chen J. Supramolecular nano-assemblies with tailorable surfaces: recyclable hard templates for engineering hollow nanocatalysts. *Sci China Mater*, 2014, 57: 7–12
9 Zhong C, Liu J, Ni Z, Deng Y, Chen B, Hu W. Shape-controlled synthesis of Pt-Ir nanocubes with preferential (100) orientation and their unusual enhanced electrocatalytic activities. *Sci China Mater*, 2014, 57: 13–25
10 Jaramillo T, Jørgensen K, Bonde J, Nielsen J, Horch S, Chorkendorff I. Identification of active edge sites for electrochemical H_2 evolution from MoS_2 nanocatalysts. *Science*, 2007, 317: 100–102
11 Zhang J, Huang K, Si W, Wu X, Cheng G, Feng S. Novel internal photoemission in manganite/ZnO heterostructure. *Sci China Chem*, 2013, 56: 583–587
12 Zhao Y, Zhang H, Huang C, Chen S, Yu B, Xu J, Liu Z. Pd nanoparticles immobilized on graphite oxide modified with a base: highly efficient catalysts for selective hydrogenation of citral. *Sci China Chem*, 2013, 56: 203–209
13 Wang L, Yue Q, Li H, Xu S, Guo L, Zhang X, Wang H, Gao X, Wang W, Liu J, Liu P. Facet-dependent electrochemiluminescence spectrum of nanostructured ZnO. *Sci China Chem*, 2013, 56: 86–92
14 Gao Z, Tong H, Chen J, Yue S, Bai W, Zhang X, Pan Y, Shi M, Song Y. Preparation and supercapacitive performance of polyaniline covalently grafted carbon nanotubes composite material. *Acta Chim Sinica*, 2014, 72: 1175–1181
15 Talapin D, Shevchenko E, Bodnarchuk M, Ye X, Chen J, Murray C. Quasicrystalline order in self-assembled binary nanoparticle superlattices. *Nature*, 2009, 461: 964–967
16 Kibsgaard J, Chen Z, Reinecke B, Jaramillo T. Engineering the surface structure of MoS_2 to preferentially expose active edge sites for electrocatalysis. *Nat Mater*, 2012, 11: 963–969
17 Gao M, Jiang D, Sun D, Hou B, Li D. Synthesis of Ag/N-TiO_2/SBA-15 photocatalysts and photocatalytic reduction of CO_2 under visible light irradiation. *Acta Chim Sinica*, 2014, 72: 1092–1098
18 Jin Q, Pei L, Hu Y, Du J, Han X, Cheng F, Chen J. Solvo/hydrothermal preparation of MnO_x@rGO nanocomposites for electrocatalytic oxygen reduction. *Acta Chim Sinica*, 2014, 72: 920–926
19 Huang M, Mao S, Feick H, Yan H, Wu Y, Kind H, Weber E, Russo R, Yang P. Room-temperature ultraviolet nanowire nanolasers. *Science*, 2001, 292: 1897–1899
20 Liang Y, Li Y, Wang H, Zhou J, Wang J, Reiger T, Dai H. Co_3O_4 nanocrystals on graphene as a synergistic catalyst for oxygen reduction reaction. *Nat Mater*, 2011, 10: 780–786
21 He P, Xu B, Wang P, Liu H, Wang X. A monolayer polyoxometalate superlattice. *Adv Mater*, 2014, 26: 4339–4344
22 Zhang Z, Xu X, Zhang J, Xiang G, Xu B, He P, Nosheen F, Saleem F, Wang X. Well-defined metal-organic framework hollow nanocages. *Angew Chem Int Ed*, 2014, 53: 429–433
23 Saleem F, Zhang Z, Xu B, Xu X, He P, Wang X. Ultrathin Pt-Cu nanosheets and nanocones. *J Am Chem Soc*, 2013, 135: 18304–18307
24 Hu S, Wang X. Ultrathin nanostructures: smaller size with new phenomena. *Chem Soc Rev*, 2013, 42: 5577–5594
25 Xu B, He P, Liu H, Wang P, Zhou G, Wang X. 1D-2D helical CdS-$ZnIn_2S_4$ hetero-nanostructure. *Angew Chem Int Ed*, 2014, 53: 2339–2343
26 Zhang J, Yang Y, Zhang Z, Wang P, Wang X. Biomimetic multifunctional nanochannels based on the asymmetric wettability of heterogeneous nanowire membrane. *Adv Mater*, 2014, 26: 1071–1075
27 Zhang J, Yang Y, Zhang Z, Xu X, Wang X. Rapid synthesis of mesoporous hollow $NixCo_{3-x}(PO_4)_2$ shells showing enhanced electrocatalytic and surpercapacitor performances. *J Mater Chem A*, 2014, 2: 20182–20188
28 Xiang G, Long Y, He J, Xu B, Liu H, Wang X. Unusual enrichment and assembly of TiO_2 nanocrystals at water/hydrophobic interfaces in a pure inorganic phase. *Langmuir*, 2014, 30: 617–623
29 Li H, Xin B, Feng L, Hao J. Stable ZnO/ionic liquid hybrid materials: novel dual-responsive superhydrophobic layers to light and anions. *Sci China Chem*, 2014, 57: 1002–1009
30 Feng R, Wang L, Lyu Z, Wu Q, Yang L, Wang X, Hu Z. Carbon nanocages supported $LiFePO_4$ nanoparticles as high-performance cathode for lithium ion batteries. *Acta Chim Sinica*, 2014, 72: 653–657
31 Liu J, Xu J, Liu Z, Liu X, Che R. Hierarchical magnetic core-shell nanostructures for microwave absorption: synthesis, microstructure and property studies. *Sci China Chem*, 2014, 57: 3–12
32 Zhang K, Hu Z, Tao Z, Chen J. Inorganic & organic materials for rechargeable Li batteries with multi-electron reaction. *Sci China Mater*, 2014, 57: 42–58
33 Li Y. Nanoparticle chemistry upgrades catalytic interfaces in noble metal catalysts. *Sci China Chem*, 2014, 7: 924–925
34 Wen L, Liu C, Song R, Luo H, Shi Y, Li F, Cheng H. Lithium storage characteristics and possible applications of graphene materials. *Acta Chim Sinica*, 2014, 72: 333–344
35 Xu B, Yang H, Zhou G, Wang X. Strong metal-support interactions in size-controlled monodisperse palladium-hematite nanoheterostructures during a liquid-solid heterogeneous catalysis. *Sci China Mater*, 2014, 57: 34–41
36 Chen C, Long M, Wu H, Cai W. One-step synthesis of Pt nanoparticles/reduced graphene oxide composite with enhanced electrochemical catalytic activity. *Sci China Chem*, 2013, 56: 354–361
37 Hou Y, Wu T, Wang L, Feng P. Integration of supertetrahedral cluster with reduced graphene oxide sheets for enhanced photostability and photoelectrochemical properties. *Sci China Chem*, 2013, 56: 423–427
38 Xu X, Lu Y, Yang Y, Nosheen F, Wang X. Tuning the growth of metal-organic framework nanocrystals by using polyoxometalates as coordination modulators. *Sci China Mater*, 2015, 58: 370–377
39 Zhang C, Yang Q. Packing sulfur into carbon framework for high volumetric performance lithium-sulfur batteries. *Sci China Mater*, 2015, 58: 349–354
40 Liu W, Qu Y, Zhou W, Ren Z, Jiang B, Wang G, Jiang L, Yuan F, Fu H. A versatile salicylic acid precursor method for preparing titanate microspheres. *Sci China Mater*, 2015, 58: 106–113
41 Deng X, Liu X, Yan H, Wang D, Wan L. Morphology and modulus evolution of graphite anode in lithium ion battery: an *in situ* AFM investigation. *Sci China Chem*, 2014, 57: 178–183
42 Zhang X, Zeng Q, Wang C. Host-guest supramolecular chemistry at solid-liquid interface: an important strategy for preparing two-dimensional functional nanostructures. *Sci China Chem*, 2014, 57: 13–25
43 Wang X, Li B, Liu D, Xiong H. $ZnWO_4$ nanocrystals/reduced graphene oxide hybrids: synthesis and their application for Li ion batteries. *Sci China Chem*, 2014, 57: 122–126

44 Yu J, Guo W, Yang M, Luan Y, Tao J, Zhang X. Synthesis of hierarchical polystyrene/polyaniline@Au nanostructures of different surface states and studies of their catalytic properties. *Sci China Chem*, 2014, 57: 1211–1217
45 Novoselov K, Geim A, Morozov S, Jiang D, Zhang Y, Dubonos S, Grigorieva I, Firsov A. Electric field effect in atomically thin carbon films. S*cience*, 2004, 306: 666–669
46 Novoselov K, Geim A, Morozov S, Jiang D, Katsnelson M, Grigorieva V, Dubonos S, Firsov A. Two-dimensional gas of massless dirac fermions in graphene. *Nature*, 2005, 438: 197–200
47 Geim A, Novoselov K. The rise of graphene. *Nat Mater*, 2007, 6: 183–191
48 Geim A, Grigorieva I. Van Der Waals heterostructures. *Nature*, 2013, 499: 419–425
49 Huang X, Zeng Z, Zhang H. Metal dichalcogenide nanosheets: preparation, properties and applications. *Chem Soc Rev*, 2013, 42: 1934–1946
50 Gong Y, Lin J, Wang X, Shi G, Lei S, Lin Z, Zou X, Ye G, Vajtai R, Yakobson B, Terrones H, Terrones M, Tay B, Lou J, Pantelides S, Liu Z, Zhou W, Ajayan P. Vertical and in-plane heterostructures from WS_2/MoS_2 monolayers. *Nat Mater*, 2014, 13: 1135–1142
51 Zhang Q, Xiao X, Zhao R, Lv D, Xu G, Lu Z, Sun L, Lin S, Gao X, Zhou J, Jin C, Ding F, Jiao L. Two-dimensional layered heterostructures synthesized from core-shell nanowires. *Angew Chem Int Ed*, 2015, 54: 8957–8960
52 Kastner M, Birgeneau R, Shirane G, Endoh Y. Magnetic, transport, and optical properties of monolayer copper oxides. *Rev Mod Phys*, 1998, 70: 897–928
53 Weller T, Ellerby M, Saxena S, Smith R, Skipper N. Super-conductivity in the intercalated graphite compounds C_6Yb and C_6Ca. *Nat Phys*, 2005, 1: 39–41
54 Ponomarenko L, Geim A, Zhukov A, Jalil R, Morozov S, Novoselov K, Grigorieva I, Hill E, Cheianov V, Fal'ko V, Watanabe K, Taniguchi T, Gorbachev R. Tunable metal-insulator transition in double-layer graphene heterostructures. *Nat Phys*, 2011, 7: 958–961
55 Vogt P, De Padova P, Quaresima C, Avila J, Frantzeskakis E, Asensio M, Resta A, Ealet B, Lay G. Silicene: compelling experimental evidence for graphenelike two-dimensional silicon. *Phys Rev Lett*, 2012, 108: 155501
56 Xu M, Liang T, Shi M, Chen H. Graphene-like two-dimensional materials. *Chem Rev*, 2013, 113: 3766–3798
57 Yan K, Fu L, Peng H, Liu Z. Designed cvd growth of graphene via process engineering. *Accounts Chem Res*, 2013, 46: 2263–2274
58 Zeng Z, Yin Z, Huang X, Li H, He Q, Lu G, Boey F, Zhang H. Single-layer semiconducting nanosheets: high-yield preparation and device fabrication. *Angew Chem Int Ed*, 2011, 50: 11093–11097
59 Rao C, Sood A, Subrahmanyam K, Govindaraj A. Graphene: the new two-dimensional nanomaterial. *Angew Chem Int Ed*, 2009, 48: 7752–7777
60 Chang K, Chen W, Ma L, Li H, Li H, Huang F, Xu Z, Zhang Q, Lee J. Graphene-like MoS_2/amorphous carbon composites with high capacity and excellent stability as anode materials for lithium ion batteries. *J Mater Chem*, 2011, 21: 6251–6257
61 Schniepp H, Li J, McAllister M, Sai H, Alonso M, Adamson D, Prud'homme R, Car R, Saville D, Aksay I. Functionalized single graphene sheets derived from splitting graphite oxide. *J Phys Chem B*, 2006, 110: 8535–8539
62 Yang X, Zhu J, Qiu L, Li D. Bioinspired effective prevention of restacking in multilayered graphene films: towards the next generation of high-performance supercapacitors. *Adv Mater*, 2011, 23: 2833–2838
63 Tang Z, Shen S, Zhuang J, Wang X. Noble-metal-promoted three-dimensional macroassembly of single-layered graphene oxide. *Angew Chem*, 2010, 122: 4707–4711
64 Wang P, Sun H, Ji Y, Li W, Wang X. Three-dimensional assembly of single-layered MoS_2. *Adv Mater*, 2014, 26: 964–969
65 Yang Y, Wang S, Zhang J, Li H, Tang Z, Wang X. Nanosheet-assembled mose 2 and S-doped mose 2–*x* nanostructures for superior lithium storage properties and hydrogen evolution reactions. *Inorg Chem Front*, 2015, 2: 931–937
66 Wang P, Li H, Liu H, He P, Xu B, Wang X. Zinc sulfide nanosheet-based hybrid superlattices with tunable architectures showing enhanced photoelectrochemical properties. *Small*, 2015, 11: 3909–3915
67 Xu Y, Sheng K, Li C, Shi G. Self-assembled graphene hydrogel via a one-step hydrothermal process. *ACS Nano*, 2010, 4: 4324–4330
68 Yavari F, Chen Z, Thomas A, Ren W, Cheng H, Koratkar N. High sensitivity gas detection using a macroscopic three-dimensional graphene foam network. *Sci Rep*, 2011, 1: 166–170
69 Cong H, Chen J, Yu S. Graphene-based macroscopic assemblies and architectures: an emerging material system. *Chem Soc Rev*, 2014, 43: 7295–7325
70 Li C, Shi G. Three-dimensional graphene architectures. *Nanoscale*, 2012, 4: 5549–5563
71 Nardecchia S, Carriazo D, Ferrer M, Gutierrez M, Monte F. Three dimensional macroporous architectures and aerogels built of carbon nanotubes and/or graphene: synthesis and applications. *Chem Soc Rev*, 2013, 4: 794–830
72 Wang Q, Kalantar-Zadeh K, Kis A, Coleman J, Strano M. Electronics and optoelectronics of two-dimensional transition metal dichalcogenides. *Nat Nanotechnol*, 2012, 7: 699–712
73 Radisavljevic B, Radenovic A, Brivio J, Giacometti V, Kis A. Single-layer MoS_2 transistors. *Nat Nanotechnol*, 2011, 6: 147–150
74 Wang X, Feng H, Wu Y, Jiao L. Controlled synthesis of highly crystalline MoS_2 flakes by chemical vapor deposition. *J Am Chem Soc*, 2013, 135: 5304–5307
75 Duan X, Wang C, Shaw J, Cheng R, Chen Y, Li H, Wu X, Tang Y, Zhang Q, Pan A, Jiang J, Yu R, Huang Y, Duan X. Lateral epitaxial growth of two-dimensional layered semiconductor heterojunctions. *Nat Nanotechnol*, 2014, 9: 1024–1030
76 Zhang L, Wu H, Yan Y, Wang X, Lou X. Hierarchical MoS_2 microboxes constructed by nanosheets with enhanced electrochemical properties for lithium storage and water splitting. *Energy Environ Sci*, 2014, 7: 3302–3306
77 Ding S, Zhang D, Chen J, Lou X. Facile synthesis of hierarchical MoS_2 microspheres composed of few-layered nanosheets and their lithium storage properties. *Nanoscale*, 2012, 4: 95–98
78 Zhuo S, Xu Y, Zhao W, Zhang J, Zhang B. Hierarchical nanosheet-based MoS_2 nanotubes fabricated by an anion-exchange reaction of MoO_3-amine hybrid nanowires. *Angew Chem*, 2013, 125: 8764–8768
79 Zhang L, Lou X. Hierarchical MoS_2 shells supported on carbon spheres for highly reversible lithium storage. *Chem-Eur J*, 2014, 20: 5219–5223
80 Lu Z, Zhu W, Yu X, Zhznag H, Li Y, Sun X, Wang X, Wang H, Wang J, Luo J, Lei X, Jiang L. Ultrahigh hydrogen evolution performance of under-water "superaerophobic" MoS_2 nanostructured electrodes. *Adv Mater*, 2014, 26: 2683–2687
81 Li Y, Wang H, Xie L, Liang Y, Hong G, Dai H. MoS_2 nanoparticles grown on graphene: an advanced catalyst for the hydrogen evolution reaction. *J Am Chem Soc*, 2011, 133: 7296–7299